Chinese Chemical Letters 32 (2021) 3221–3225

Contents lists available at ScienceDirect

Chinese Chemical Letters

journal homepage: www.elsevier.com/locate/cclet

Communication

Electro-catazone treatment of an ozone-resistant drug: Effect of sintering temperature on TiO_2 nanoflower catalyst on porous Ti gas diffuser anodes

Xinyang Li[a], Yannan Li[a], Hao Zhang[a], Zhen Shen[a], Shuang Cheng[a], Guicheng Liu[b], Hong Yao[a,*]

[a] Beijing International Scientific and Technological Cooperation Base of Water Pollution Control Techniques for Antibiotics and Resistance Genes, Beijing Key Laboratory of Aqueous Typical Pollutants Control and Water Quality Safeguard, Department of Municipal and Environmental Engineering, School of Civil Engineering, Beijing Jiaotong University, Beijing 100044, China
[b] Department of Physics, Dongguk University, Seoul 04620, Republic of Korea

ARTICLE INFO

Article history:
Received 28 December 2020
Received in revised form 6 February 2021
Accepted 26 March 2021
Available online 30 March 2021

Keywords:
Electrochemical
Ozonation
Sintering temperature
Crystallized phase
Interface reactions

ABSTRACT

Electrochemical heterogeneous catalytic ozonation (E-catazone) is a promising and advanced oxidation technology that uses a titanium dioxide nanoflower ($TiO_{2\text{-}NF}$)-coated porous Ti gas diffuser as an anode material. Our previous study has highlighted that the importance of the $TiO_{2\text{-}NF}$ coating layer in enhancing $^{\bullet}OH$ production and rapidly degrading O_3-resistant drugs. It is well known that the properties of $TiO_{2\text{-}NF}$ are closely related to its sintering temperature. However, to date, related research has not been conducted in E-catazone systems. Thus, this study evaluated the effect of the sintering temperature on the degradation of the O_3-resistant drug *para*-chlorobenzoic acid (*p*-CBA) using both experimental and kinetic modeling and revealed its influence mechanism. The results indicated that the $TiO_{2\text{-}NF}$ sintering temperature could influence *p*-CBA degradation and $^{\bullet}OH$ production. $TiO_{2\text{-}NF}$ prepared at 450 °C showcased the highest *p*-CBA removal efficiency (98.5% in 5 min) at a rate of 0.82 min^{-1}, and an $^{\bullet}OH$ exposure of 8.41×10^{-10} mol L^{-1} s. Kinetic modeling results and interface characterization data revealed that the sintering temperature could alter the TiO_2 crystallized phase and the content of surface-adsorbed oxygen, thus affecting the two key limiting reactions in the E-catazone process. That is, $\equiv TiO_2$ surface reacted with H_2O to form TiO_2-$(OH)_2$, which then heterogeneously catalyzed O_3 to form $^{\bullet}OH$. Consequently, E-catazone with a $TiO_{2\text{-}NF}$ anode prepared at 450 °C generated the highest surface reaction rate (5.00×10^{-1} s^{-1} and 4.00×10^{-3} L mol^{-1} s^{-1}, respectively), owing to its higher anatase content and adsorbed oxygen. Thus, a rapid O_3-TiO_2 reaction was achieved, resulting in an enhanced $^{\bullet}OH$ formation and a highly effective *p*-CBA degradation. Overall, this study provides novel baseline data to improve the application of E-catazone technology.

In recent years, the electrocatalytic ozonation process has received widespread attention because of its highly efficient removal of pharmaceutical micropollutants [1–5]. In 2016, a new electrocatalytic ozonation process was developed by our research group, namely: Electrochemical heterogeneous catalytic ozonation (E-catazone); this as achieved by using a self-made titanium dioxide nanoflower coated porous Ti gas diffuser ($TiO_{2\text{-}NF}$@PTGD) as the anode [6], and carbon-coated electrode as the cathode. Owing to the integration of an ozone aerator, ozone catalyst, and anode into $TiO_{2\text{-}NF}$@PTGD, O_3 was transferred to the surface of porous titanium under forced convection and subsequently converted into reactive oxygen species (ROS) under the action of electrochemistry and the $TiO_{2\text{-}NF}$ catalytic layer. Thus, the E-catazone process resulted in a hydroxyl radical production that was two orders of magnitude greater than that obtained using electrochemical oxidation and ozonation alone. Furthermore, this process exhibits excellent mass transfer and oxidation characteristics, while demonstrating great potential for the fast and effective degradation of ozone-resistant micropollutants [7,8]. Our previous study has confirmed that the $TiO_{2\text{-}NF}$ catalyst layer on the porous Ti anode plays an important role in the augmented pollutant removal and enhances the generation of ROS in E-catazone [7]. Notably, the $TiO_{2\text{-}NF}$ not only promotes the interface reaction with the H_2O surface under an electrochemical action (Eq. 1), but also improves

* Corresponding author.
E-mail addresses: hyao@bjtu.edu.cn, yaohongts@163.com (H. Yao).

https://doi.org/10.1016/j.cclet.2021.03.072
1001-8417/

the interface adsorption of O_3 and its subsequent conversion into ROS (Eq. 2):

$$\equiv TiO_2 + 2\ H_2O \rightarrow \equiv TiO_2\text{-}(OH)_2 + 2H^+ + 2e^- \quad (1)$$

$$\equiv TiO_2\text{-}(OH)_2 + O_3 \rightarrow \equiv TiO_2 + 2O + {}^{\bullet}OH + HO_2^{\bullet} \quad (2)$$

The morphology, hierarchical structure, and crystal form of the catalyst play a vital role in its catalytic ability [9–11]. $TiO_{2\text{-}NF}$ exhibits a three-dimensional [12,13], hierarchical, and porous structure [14] that provides sufficient interface area for gas/solid/bulk solution reactions to occur [13,15]. The $TiO_{2\text{-}NF}$ coating is prepared in situ and grown on the porous titanium substrate using the alkaline hydrothermal method; subsequently it is crystallized by sintering at a temperature of 450 °C [6]. It is well known that the sintering temperature can significantly affect the crystal form of TiO_2 [16], which in turn affects its catalytic activities. At a sintering temperature of lower than 500 °C, TiO_2 predominantly takes the form of anatase, and an increase in temperature gradually transforms the anatase into rutile [17]. In our previous studies, we have determined that $TiO_{2\text{-}NF}$@PTGD prepared at a sintering temperature of 450 °C exists in the form of anatase and produces excellent catalytic effects in the E-catazone system [6–8]. Moreover, Song *et al*. [18] prepared different crystal types of nano-TiO_2 by altering the sintering temperature and found that the anatase phase of TiO_2 prepared at 450 °C displayed better catalytic activities than those of rutile TiO_2 prepared at a temperature of 750 °C, while also exhibiting a higher specific surface area. Such results can be explained by the fact that anatase TiO_2 has a higher surface hydroxyl density than that of rutile TiO_2, and that surface hydroxyl groups are major reaction sites for the interfacial catalysis of O_3 and TiO_2. In previous E-catazone studies, there has been no systematic evaluation of the preparation process parameters of TiO_2 and it is not clear whether the sintering temperature of TiO_2 affected the catalytic performance of TiO_2-O_3 and the degradation efficiency of refractory organic compounds. Furthermore, it has been noted that the effective removal of ozone-resistant drugs is essential for the control of pharmaceutical micropollutants. Therefore, in the present study, an ozone-resistant drug with a second-order reaction kinetic constant of $k_{p\text{-CBA,O3}} < 1\ L\ mol^{-1}\ s^{-1}$ was chosen as the target pollutant, namely, *para*-chlorobenzoic acid (*p*-CBA) [19–21]. The effects of preparing $TiO_{2\text{-}NF}$@PTGDs at different sintering temperatures on the degradation of *p*-CBA by E-catazone were investigated by analyzing the physical characteristics of $TiO_{2\text{-}NF}$ and the degradation characteristics of *p*-CBA. The influence mechanism was also revealed by analyzing interfacial reaction kinetics, measuring the exposure of hydroxyl radicals, and simulating the O_3-TiO_2 interface reaction characteristics *via* kinetic modeling methods. The details of the experiment have been listed in the supporting information, including the preparation and characterization of $TiO_{2\text{-}NF}$@PTGDs, E-catazone treatment of *p*-CBA, hydroxyl radical exposure, and kinetic modeling.

The $TiO_{2\text{-}NF}$ coatings were all uniformly grown on the porous titanium substrate. The morphologies of $TiO_{2\text{-}NF}$@PTGDs prepared without sintering ($TiO_{2\text{-}NF}$@PTGD-ws), and at sintering temperatures of 350 °C ($TiO_{2\text{-}NF}$@PTGD-350), 450 °C ($TiO_{2\text{-}NF}$@PTGD-450), and 550 °C ($TiO_{2\text{-}NF}$@PTGD-550) were similar, with $TiO_{2\text{-}NF}$ comprising multiple TiO_2 nanosheets arranged in an array (Figs. 1a–d and f–i). Notably, the morphology of the $TiO_{2\text{-}NF}$@PTGD prepared at 750 °C ($TiO_{2\text{-}NF}$@PTGD-750) was slightly different. That is, the TiO_2 nanosheets took the form of nanorod arrays (Figs. 1e and j) because the nanosheets were broken at higher temperatures and subsequently exhibited rod shapes. Furthermore, the XRD data of $TiO_{2\text{-}NF}$@PTGDs at different sintering temperatures indicated that the $TiO_{2\text{-}NF}$@PTGD surface layers exhibited a crystal structure (Fig. S1 in Supporting information). The crystallite phase composition of $TiO_{2\text{-}NF}$@PTGDs was analyzed using the JADE.6 software. Results highlighted that variations in the sintering temperature significantly affected the surface crystal composition of $TiO_{2\text{-}NF}$@PTGDs (Table 1). For $TiO_{2\text{-}NF}$@PTGD-ws, the surface was mainly composed of Ti_8O_{15} (Table 1). In contrast, the surfaces of $TiO_{2\text{-}NF}$@PTGD-350, $TiO_{2\text{-}NF}$@PTGD-450, and $TiO_{2\text{-}NF}$@PTGD-550 were mainly composed of anatase TiO_2 and titanium matrix, and the sintering temperature affected the proportion of anatase TiO_2 (Table 1). When the sintering temperature increased from 350 °C to 450 °C, the mass proportion of anatase TiO_2 increased from 69.1% to 81.2%; however, as temperature increased to 550 °C, the value gradually decreased to 79.3%. Finally, as the temperature further increased to 750 °C, the proportion of anatase TiO_2 decreased to 7.2%, and the proportion of rutile TiO_2 reached 70.6%; this indicates that anatase TiO_2 transforms to rutile TiO_2 at high temperatures. Notably, this trend is similar to that reported in other studies [22,23].

The XPS spectra of the O 1s bands in the 529–535 eV binding energy region for all the prepared $TiO_{2\text{-}NF}$@PTGD samples are displayed in Fig. 2 and Fig. S2 in Supporting information. Except for that of $TiO_{2\text{-}NF}$@PTGD-750, all spectra could be fitted into two O 1s peaks, 529.4–530.3 eV [24] and 531.7–532.3 eV [25], which corresponded to the metallic oxides (*i.e*., lattice oxygen [O_L] of the $TiO_{2\text{-}NF}$) [26] and adsorbed surface oxygen groups (O_{ads}) such as ≡OH or other hydrated species [26], respectively. These are major reaction sites for heterogeneous catalytic reactions of O_3. The peak area data for both O_L and O_{ads} are listed in Table 1. Interestingly, the O_{ads} values indicated that our self-made

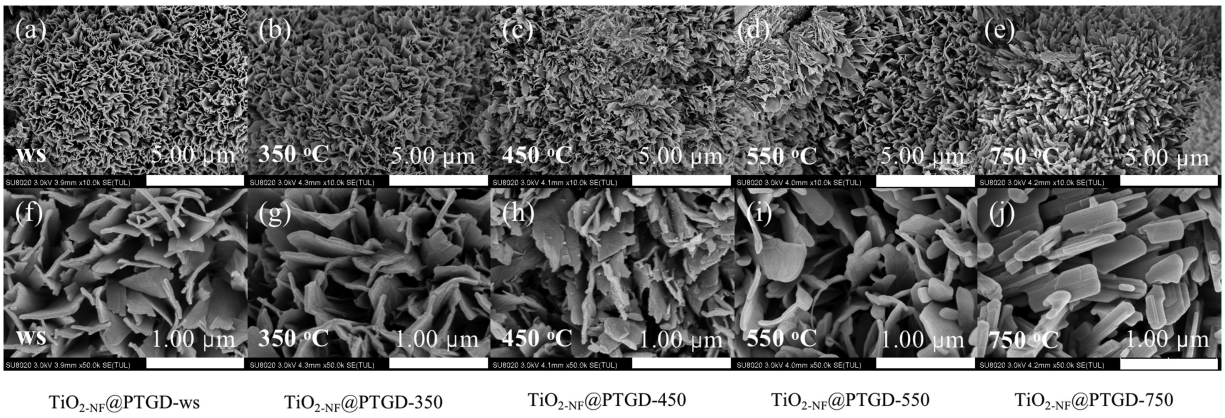

Fig. 1. Morphologies of nanoflower-shaped titanium oxide-coated porous Ti gas diffusers prepared at different sintering temperatures. The diffusers were prepared without sintering (a, f), and at sintering temperatures of 350 °C (b, g), 450 °C (c, h), 550 °C (d, i) and 750 °C (e, j), respectively.

Table 1
Physicochemical parameters and observed *pseudo*-first-order kinetic constant (k_{obs}) for *p*-CBA degradation by E-catazone with different nanoflower-shaped titanium oxide-coated porous Ti gas diffuser ($TiO_{2\text{-}NF}$@PTGD) anodes.

Sintering temperature	Sample	Crystallite phase (%, wt% by mass)	O_{ads} peak area (a. u.)	O_L peak area (a. u.)	k_{obs} ($\times 10^{-1}$ min^{-1})
Without sintering	$TiO_{2\text{-}NF}$@PTGD-ws	Ti_8O_{15} (98.0), Ti (2.0)	6.60×10^3	1.01×10^4	2.82
350 °C	$TiO_{2\text{-}NF}$@PTGD-350	anatase (69.1), Ti (30.9)	8.32×10^3	2.55×10^4	6.05
450 °C	$TiO_{2\text{-}NF}$@PTGD-450	anatase (81.2), Ti (18.8)	1.26×10^4	2.32×10^4	8.20
550 °C	$TiO_{2\text{-}NF}$@PTGD-550	anatase (79.3), Ti (20.7)	1.23×10^4	2.55×10^4	3.92
750 °C	$TiO_{2\text{-}NF}$@PTGD-750	anatase (7.2), rutile (70.6), Ti (22.2)	0	2.50×10^5	0.38

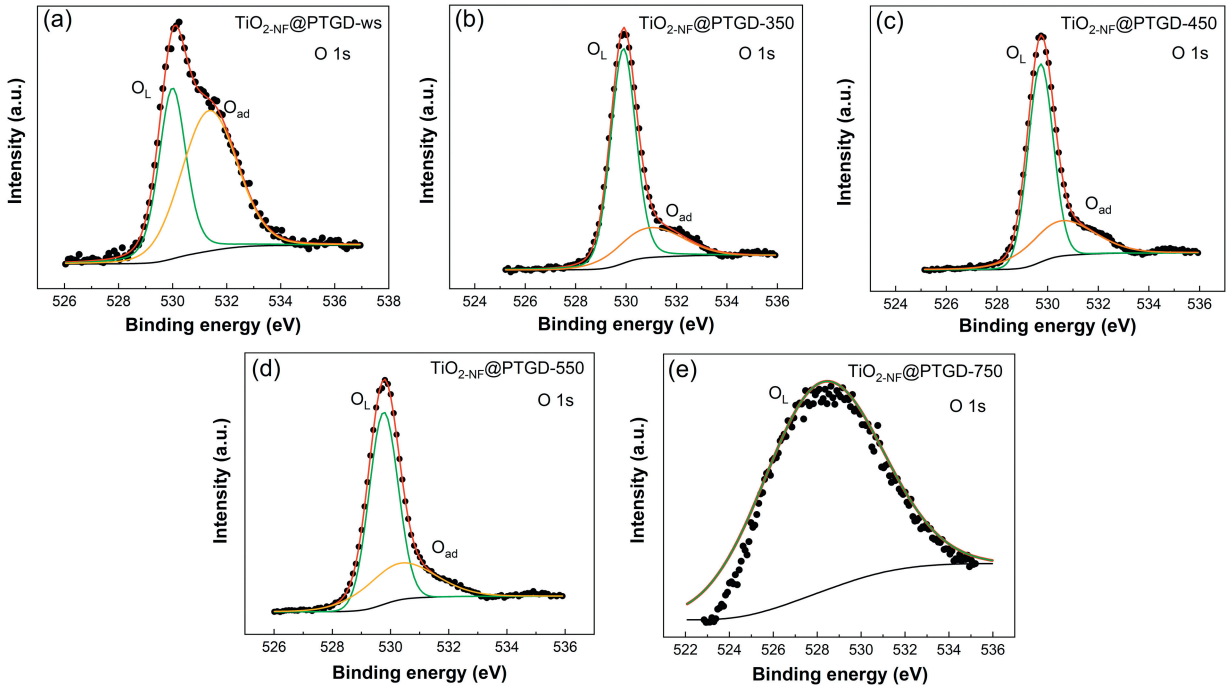

Fig. 2. XPS spectra of O 1s on the surface of nanoflower-shaped titanium oxide-coated porous Ti gas diffusers ($TiO_{2\text{-}NF}$@PTGDs) without sintering ($TiO_{2\text{-}NF}$@PTGD-ws) (a); at 350 °C ($TiO_{2\text{-}NF}$@PTGD-350) (b); 450 °C ($TiO_{2\text{-}NF}$@PTGD-450) (c); 550 °C ($TiO_{2\text{-}NF}$@PTGD-550) (d); 750 °C ($TiO_{2\text{-}NF}$@PTGD-750) (e).

$TiO_{2\text{-}NF}$@PTGD at the sintering temperature of 450 °C may comprise more surface oxygen sites during the interfacial catalysis of O_3; therefore, it can react with O_3 and convert it to ROS more effectively, as compared to other $TiO_{2\text{-}NF}$@PTGDs.

The sintering temperature of $TiO_{2\text{-}NF}$@PTGD can remarkably influence *p*-CBA degradation (Figs. 3a and b). When the sintering temperature increased from room temperature to 450 °C, *p*-CBA removal increased from 69.6% to 98.5% within 5 min. Notably, the *p*-CBA degradation curves were fitted with the pseudo-first-order kinetic characteristics and *p*-CBA removal rates. Further, the *pseudo*-first-order removal rate constant $k_{p\text{-CBA}}$ increased by a magnitude of 2.91, from 2.82×10^{-1} min^{-1} to 8.20×10^{-1} min^{-1} (Table 1). However, when the sintering temperature was further increased to 750 °C, the *p*-CBA removal efficiency after 5 min and $k_{p\text{-CBA}}$ were decreased to 15.9% and 3.8×10^{-2} min^{-1}, respectively. The same trend was also observed in the hydroxyl radical exposure ($\int$[$^{\bullet}$OH]dt) obtained with different $TiO_{2\text{-}NF}$@PTGDs. As the sintering temperature increased to 450 °C, the $\int$[$^{\bullet}$OH] dt obtained for $TiO_{2\text{-}NF}$@PTGD-450 increased from 2.38×10^{-10} mol L^{-1} s to 8.41×10^{-10} mol L^{-1} s; however, $\int$[$^{\bullet}$OH] dt rapidly decreased to 3.45×10^{-11} mol L^{-1} s for $TiO_{2\text{-}NF}$@PTGD-750 when the sintering temperature further rose to 750 °C (Figs. 3c and d). The positive correlation between the $\int$[$^{\bullet}$OH] dt and the degradation of p-CBA indicates that the sintering temperature of $TiO_{2\text{-}NF}$@PTGDs influences the degradation of *p*-CBA by affecting the $\int$[$^{\bullet}$OH]dt of E-catazone. *p*-CBA is a typical ozone-inert drug, therefore, it can hardly be oxidized by O_3 alone but can be effectively degraded by $^{\bullet}$OH. Therefore, the rapid degradation of *p*-CBA in E-catazone is closely related to the excellent interface properties of the $TiO_{2\text{-}NF}$@PTGD-450 electrode and its ability to produce $^{\bullet}$OH. Finally, the highest content of O_{ads} for $TiO_{2\text{-}NF}$@PTGD was obtained at the sintering temperature of 450 °C, which indicates that the $TiO_{2\text{-}NF}$@PTGD-450 contained the highest amount of surface oxygen groups; therefore, it functioned as a reaction site for the catalysis of molecular O_3 into ROS [27,28].

As indicated in our previous study [7], the O_3 interface catalytic process of $TiO_{2\text{-}NF}$@PTGD in E-catazone mainly involves the reaction of $TiO_{2\text{-}NF}$ with water molecules under an electrochemical action to produce surface oxygen groups (Eq. 1), as well as the interface conversion between hydroxylated $TiO_{2\text{-}NF}$ and O_3 to produce ROS (Eq. 2).

These two reactions are the important rate-limiting steps for the catalytic conversion of ozone to produce ROS and promote the rapid degradation of organic compounds. To further analyze the effects of the TiO_2 sintering temperature on the reaction rate of the limiting reactions, the kinetic model of the E-catazone reaction system was established using the Kintecus software (V6.80). By fitting the degradation curves of *p*-CBA (Fig. S3 in Supporting information), the kinetic rate constants of Eqs. 1 ($k_{Eq.1}$) and 2 ($k_{Eq.2}$) were obtained. The sintering temperature of $TiO_{2\text{-}NF}$@PTGD significantly influenced the reaction rates, $k_{Eq.1}$ and $k_{Eq.2}$ (Fig. 4). At the sintering temperature of 450 °C, $TiO_{2\text{-}NF}$@PTGD-450

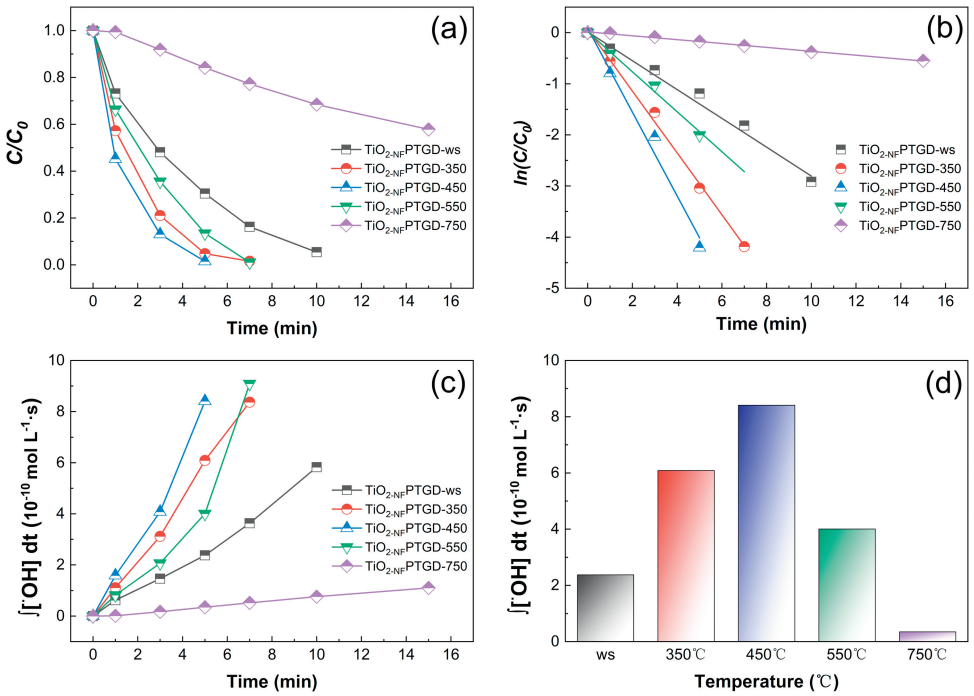

Fig. 3. Removal of *p*-CBA (a), *pseudo*-first-order kinetic constant (k_{obs}) of *p*-CBA degradation (b), evolution of hydroxyl radical exposure ($\int[^{\bullet}OH]\,dt$) with reaction time (c), and hydroxyl radical exposure ($\int[^{\bullet}OH]\,dt$) at 5 min (d) in E-catazone system using different nanoflower-shaped titanium oxide-coated porous Ti gas diffusers ($TiO_{2\text{-}NF}$@PTGDs). Experimental conditions: *p*-CBA concentration of 8 mg/L; current of 150 mA; gas flow rate of 0.2 L min^{-1}; O_3 concentration of 10 mg/L; and an initial pH of 7.2.

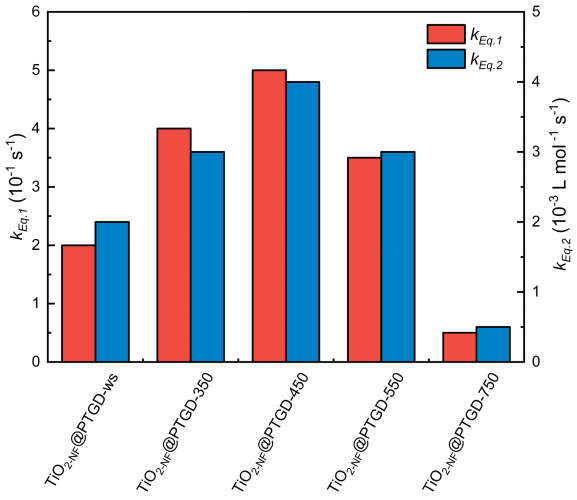

Fig. 4. Kinetic rate constants of two key TiO_2-O_3 interface reactions with different nanoflower-shaped titanium oxide-coated porous Ti gas diffusers ($TiO_{2\text{-}NF}$@PTGDs).

exhibited $k_{Eq.1}$ and $k_{Eq.2}$ values of 5.00×10^{-1} s^{-1} and 4.00×10^{-3} L mol^{-1} s^{-1}, respectively, which were much higher than those of $TiO_{2\text{-}NF}$@PTGD-ws (2.00×10^{-1} s^{-1} and 2.00×10^{-3} L mol^{-1} s^{-1}) and $TiO_{2\text{-}NF}$@PTGD-750 (5.00×10^{-2} s^{-1} and 5.00×10^{-4} L mol^{-1} s^{-1}) (Table S1 in Supporting information).

Interestingly, we found that the effect of the sintering temperature on the interfacial reaction rate was the same as that of O_{ads} and hydroxyl radical exposure. The sintering temperature affects the crystal type and content of $TiO_{2\text{-}NF}$ and controls the content of O_{ads} on the surface of $TiO_{2\text{-}NF}$, thereby causing $TiO_{2\text{-}NF}$ to exhibit different surface energies [29]. In the E-catazone system, the electrochemical action can further promote the reaction of the $TiO_{2\text{-}NF}$ interface with water molecules to form surface-active groups such as $\equiv TiO_2\text{-}(OH)_2$ [7,30,31]. This active group is rich in electrons and can be enhanced and induced by electrostatic forces to ensure that ozone molecules are adsorbed on the interface of TiO_2. In the present study, the adsorbed ozone was further catalyzed and formed surface atomic oxygen (O) or $HO_2^{\bullet}$. These ROS were then converted to $^{\bullet}OH$ through a series of homogeneous elementary reactions (Table S1c). Thus, $TiO_{2\text{-}NF}$@PTGD sintered at 450 °C demonstrates the highest interfacial activity to react with water molecules and catalyze O_3, converting it into ROS for the rapid degradation of pollutants. In addition, the above results indicate that E-catazone exhibits an excellent degradation efficiency for ozone inert drugs and can achieve rapid removal. This observation provides new technical means and ideas for the efficient removal of micropollutants of refractory drugs and for the effective management and control of pharmaceutical and personal care products (PPCPs).

In summary, this study demonstrated that the sintering temperature of $TiO_{2\text{-}NF}$ is the primary factor affecting the oxidation ability of the E-catazone system. The mechanism governing the influence of sintering temperature on the oxidation activity of E-catazone was revealed, and the optimum sintering temperature was defined. The results indicated that TiO_2 prepared at the sintering temperature of 450 °C was the most efficient against the ozone-inert drug *p*-CBA. The underlying explanation for this result is that the $TiO_{2\text{-}NF}$ electrode generated the highest content of both anatase and O_{ads} and had higher surface energy, thereby laying the foundation for the subsequent O_3-TiO_2 interface catalysis.

Therefore, under the electrochemical action of the TiO_2 electrode, the TiO_2 interface binds rapidly and produces active groups, which further promote the adsorption and catalytic transformation of the O_3 interface, resulting in a large amount of ROS to achieve the rapid degradation of refractory organic compounds.

Declaration of competing interest

The authors report no declarations of interest.

Acknowledgments

This research was supported by the Beijing Outstanding Young Scientist Project (No. C19H100010), Beijing Outstanding Talent Training Foundation, China (No. 2018000020124G056) with title 'Efficient removal and toxicity study of typical antibiotics from waste water of high-speed railway trains in Beijing', the National Natural Science Foundation of China (No. 52042201).

Appendix A. Supplementary data

Supplementary material related to this article can be found, in the online version, at doi:https://doi.org/10.1016/j.cclet.2021.03.072.

References

[1] K.L. Li, Y. Zhang, L.L. Xu, et al., Appl. Catal. B 264 (2020) 118512.
[2] K.L. Li, L.L. Xu, Y. Zhang, et al., Appl. Catal. B 249 (2019) 316–321.
[3] J. Li, Y. Li, Z. Xiong, G. Yao, B. Lai, Chin. Chem. Lett. 30 (2019) 2139–2146.
[4] Y.J. Wang, G. Yu, S.B. Deng, J. Huang, B. Wang, Chemosphere 208 (2018) 640–654.
[5] T. Wang, Y.Q. Song, H.J. Ding, et al., Chem. Eng. J. 394 (2020) 124852.
[6] X. Li, G. Liu, M. Shi, et al., Sep. Purif. Technol. 165 (2016) 154–159.
[7] X. Li, F. Ma, Y. Li, et al., Chem. Eng. J. 389 (2020) 124411.
[8] X. Li, S. Sun, X. Zhang, et al., Sep. Purif. Technol. 178 (2017) 189–192.
[9] J.P. Zou, Y. Chen, S.S. Liu, et al., Water Res. 150 (2019) 330–339.
[10] F. Yu, L. Wang, Q. Xing, et al., Chin. Chem. Lett. 31 (2020) 1648–1653.
[11] M. Zhu, L. Zhang, S. Liu, et al., Chin. Chem. Lett. 31 (2020) 1961–1965.
[12] Y. Wang, M.M. Zhang, S.H. Lv, et al., ACS Omega 5 (2020) 13994–14005.
[13] H.X. Li, C. Yang, X.Y. Wang, et al., J. Am. Ceram. Soc. 103 (2020) 1187–1196.
[14] X. Li, G. Liu, M. Shi, et al., Electrochim. Acta 218 (2016) 318–324.
[15] M.S. Akhtar, A. Umar, S. Sood, et al., Materials 12 (2019) 566.
[16] H. Sutrisno, E.D. Siswani, K.S. Budiasih, Sci. Sinter. 50 (2018) 291–298.
[17] A.L. Li, Z.L. Wang, H. Yin, et al., Chem. Sci. 7 (2016) 6076–6082.
[18] S. Song, Z.W. Liu, Z.Q. He, A.L. Zhang, J.M. Chen, Sci. Technol. 44 (2010) 3913–3918.
[19] R.H. Huang, J. Liu, L.S. Li, et al., Chin. Chem. Lett. 22 (2011) 683–686.
[20] J.X. Yang, J. Li, W.Y. Dong, et al., Chem. Eng. J. 295 (2016) 443–450.
[21] B.Y. Lan, R.H. Huang, L.S. Li, et al., Chem. Eng. J. 219 (2013) 346–354.
[22] D.A.H. Hanaor, C.C. Sorrell, J. Mater, Sci. Mater. Electron. 46 (2011) 855–874.
[23] G. Chen, J. Chen, Z.K. Song, C. Srinivasakannan, J.H. Peng, J. Alloys. Compd. 585 (2014) 75–77.
[24] A.R. Babar, S.S. Shinde, A.V. Moholkar, et al., J. Alloys. Compd. 509 (2011) 3108–3115.
[25] K. Srinivas, M. Vithal, B. Sreedhar, M.M. Raja, P.V. Reddy, J. Phys. Chem. C 113 (2009) 3543–3552.
[26] T. Wu, G.H. Zhao, Y.Z. Lei, P.Q. Li, J. Phys. Chem. 115 (2011) 3888–3898.
[27] C. Mansas, J. Mendret, S. Brosillon, A. Ayral, Sep. Purif. Technol. 236 (2020) 116221.
[28] J. Wang, H. Chen, Sci. Total Environ. 704 (2020) 135249.
[29] X.F. Lang, Y.H. Liang, J. Zhang, et al., Phys. Chem. Chem. Phys. 22 (2020) 1371–1380.
[30] F. Rodríguez-Hernández, D.C. Tranca, B.M. Szyja, et al., J. Phys. Chem. 120 (2016) 437–449.
[31] X. Yin, H. Wang, E.H. Han, Surf. Sci. 691 (2020) 121504.